HHS Public Access

Author manuscript

J Genet Genomics. Author manuscript; available in PMC 2017 June 20.

Published in final edited form as:

J Genet Genomics. 2016 June 20; 43(6): 381–391. doi:10.1016/j.jgg.2015.11.006.

Depletion of BBS Protein LZTFL1 Affects Growth and Causes Retinal Degeneration in Mice

Jiangsong Jiang[a,*], **Kanyarat Promchan**[a], **Hong Jiang**[a,1], **Parirokh Awasthi**[b], **Heather Marshall**[a], **Adam Harned**[c], and **Ven Natarajan**[a,*]

[a]Laboratory of Molecular Cell Biology, Leidos Biomedical Research, Inc., Frederick National Laboratory for Cancer Research, Frederick, MD 21702, USA

[b]Transgenic Mouse Model Laboratory, Leidos Biomedical Research, Inc., Frederick National Laboratory for Cancer Research, Frederick, MD 21702, USA

[c]Electron Microscopy Laboratory, Leidos Biomedical Research, Inc., Frederick National Laboratory for Cancer Research, Frederick, MD 21702, USA

Abstract

Bardet-Biedl syndrome (BBS) is a heterogeneous disease characterized by deficiencies in various organs that are caused by defects in genes involved in the genesis, structural maintenance, and protein trafficking of cilia. Leucine zipper transcription factor-like 1 (LZTFL1) has been identified as a BBS protein (BBS17) because patients with mutations in this gene exhibit the common BBS phenotypes. In this study, we generated a knockout mouse model to investigate the effects of LZTFL1 depletion. *Lztfl1* knockout mice were born with low birth weight, reached similar weight to those of wild-type mice at 10 weeks of age, and later gained more weight than their wild-type counterparts. LZTFL1 was localized to the primary cilium of kidney cells, and the absence of LZTFL1 increased the ciliary localization of BBS9. Moreover, in the retinas of *Lztfl1* knockout mice, the photoreceptor outer segment was shortened, the distal axoneme of photoreceptor connecting cilium was significantly enlarged, and rhodopsin was targeted to the outer nuclear layer. TUNEL assay showed that many of these abnormal photoreceptor cells in *Lztfl1* knockout mice underwent apoptosis. Interestingly, the absence of LZTFL1 caused an abnormal increase of the adaptor protein complex 1 (AP1) in some photoreceptor cells. Based on these data, we conclude that LZTFL1 is a cilium protein and it regulates animal weight and photoreceptor connecting cilium function probably by controlling microtubule assembly and protein trafficking in cilia.

[*]Corresponding authors. Tel: 301-846-1248 (V. Natarajan; J. Jiang) Vnatarajan@mail.nih.gov (V. Natarajan); jiangj2@mail.nih.gov (J. Jiang).

[1]Current Address: The Graduate Center for Toxicology, the Markey Cancer Center, University of Kentucky, Lexington, KY 40536, USA

Supplementary Data

Fig. S1. The evaluation of BBS9 antibody specificity for mouse tissue.

Fig. S2. Quantitation of BBS9 in the primary cilia of wild-type and *Lztfl1* knockout kidney cells.

Fig. S3. Presence of fork-like structure at the distal end of the *Lztfl1* knockout connecting cilium.

Keywords

LZTFL1; cilium; BBSome; BBS17; retina; AP-1

1. Introduction

The leucine zipper transcription factor-like 1 (*LZTFL1*) gene codes for a ubiquitously expressed cytoplasmic protein (Wei et al., 2010). It has been reported that a 5-bp deletion in the *LZTFL1* gene is associated with Bardet-Biedl syndrome (BBS) (Marion et al., 2012b). BBS phenotypes include retinal degeneration, obesity, cognitive impairment, polydactyly, hypogonadism, polyuria, polydipsia, kidney failure, and heart *situs inversus* (Kim et al., 2004; Kulaga et al., 2004; Mykytyn et al., 2004; Yen et al., 2006; Zhang et al., 2011; Marion et al., 2012a; Berbari et al., 2013; Forsythe and Beales, 2013; Schaefer et al., 2014). Since *LZTFL1* is the 17th identified gene associated with BBS, it is designated as *BBS17* (Marion et al., 2012b).

Biochemical studies have shown that LZTFL1 binds to the BBSome, a multi-protein complex containing BBS1, BBS2, BBS4, BBS5, BBS7, BBS8, and BBS9 (Jin et al., 2010; Sheffield, 2010; Seo et al., 2011). *In vitro* studies showed that LZTFL1 is associated with the BBSome through physical interaction with BBS9 (Seo et al., 2011). Because the BBSome and canonical coat complexes, such as clathrin, COPI, and COP II, share some structural features (van Dam et al., 2013), BBSome might be involved in cellular trafficking related to vesicle coating on cellular (Nachury et al., 2007; Nachury, 2014).

Primary cilium is a signaling hub for mechanical, chemical, and optical sensing (Avidor-Reiss et al., 2004; Pampliega et al., 2013; Tang et al., 2013; Nachury, 2014). Protein trafficking within the primary cilium is supported by the BBSome and the intraflagellar transport system (IFT complexes A and B), which form IFT trains moving along the microtubule (Pigino et al., 2009; Taschner et al., 2011), and BBSome can facilitate IFT assembly and turnaround in the cilium (Scholey, 2008; Taschner et al., 2011; Pedersen and Christensen, 2012; Wei et al., 2012; Bhogaraju et al., 2013; Williams et al., 2014). Previous studies have demonstrated that the knockdown and overexpression of *LZTFL1* are inversely related to BBS9 levels in the primary cilium of hTERT-RPE1 cells, while BBSome ciliary trafficking in *Bbs3* and *Bbs5* knockdown cells was restored when LZTFL1 activity was reduced (Seo et al., 2011). Based on these data, it was concluded that LZTFL1 negatively regulated BBSome trafficking to the ciliary membrane (Seo et al., 2011). Recently, Eguether et al. (2014) found that the BBSome and LZTFL1 accumulated to high levels in *Ift27* mutant cilia, while *Lztfl1* mutant cells accumulated BBSome but not IFT27, they thereby proposed that LZTFL1 functions downstream of IFT27 for coordinated removal of patched-1 and Smoothened from cilia during hedgehog signaling.

Given the complex roles of LZTFL1 in BBS, cancer, immune system, and other pathways (Kiss et al., 2001; Kang et al., 2011; Lee et al., 2011; Sakurai et al., 2011), it is vital to have an animal model to study its functions under physiological conditions. In this study, we generated a *Lztfl1* knockout mouse model and showed that it exhibits phenotypes similar to those of other *BBS* knockout mouse models, including obesity and retinal degeneration. In

Lztfl1 knockout mice, BBS9 was increased in the primary cilium of kidney cells, and the distal end of the axoneme of the photoreceptor connecting cilia in the retinas was significantly enlarged, as compared to the wild type. These physiological data should be helpful in understanding the role of LZTFL1 in its related human diseases.

2. Results

2.1 LZTFL1 depletion affects body weight in mice

The *Lztfl1* knockout mouse line was generated *via* the conventional embryonic stem (ES) cell-based gene-targeting approach, using an ES cell clone in which the *Lztfl1* gene was disrupted by inserting a DNA fragment with a *LacZ-neo* cassette between exons 3 and 4 of *Lztfl1* (Fig. 1A). The homozygous *Lztfl1* knockout mice ($Lztfl1^{-/-}$) were obtained by intercrossing heterozygous mice ($Lztfl1^{+/-}$). The absence of LZTFL1 and significantly decreased expression of *Lztfl1* in $Lztfl1^{-/-}$ mice was confirmed by Western blot and real-time quantitative RT-PCR (qRT-PCR) analyses, respectively (Fig. 1B and C). Genotyping of offspring derived from heterozygous intercrosses showed an abnormal segregation ratio ($Lztfl1^{-/-}$:$Lztfl1^{+/-}$:$Lztfl1^{+/+}$ = 1:4.3:2.3, $P < 0.001$, Chi-square test, $n = 981$), indicating a defect in the embryogenesis of the *Lztfl1*-null embryo. *Lztfl1* knockout mice were born with low birth weight, reached similar weight to wild type at 10 weeks of age, and later gained more weight than their wild-type counterparts (Fig. 2A–D). Overall, these results revealed that LZTFL1 has an effect on animal weight.

2.2 LZTFL1 localizes in the primary cilium of the kidney and regulates BBS9

To ascertain the role of LZTFL1 in cilia, kidney tissues from wild-type and knockout mice were stained with an antibody against LZTFL1 and imaged with a confocal microscope. The result showed that LZTFL1 was present as discrete speckles in the primary cilium of the wild-type kidney cells (Fig. 3A) but absent in the *Lztfl1* knockout mice (Fig. 3B). Next, cells from knockout and wild-type kidney tissues were cultured, the primary cilium was induced by serum starvation, and the localization and the level of BBS9 were examined by immunofluorescent staining with an antibody against BBS9 and imaged by confocal microscopy. Compared to wild type, knockout cells showed increased ciliary localization of BBS9 (data not shown), which is consistent with the result reported for the hTERT-RPE1 cell line (Seo et al., 2011). Similar results were seen in kidney tissue sections (Figs. 3C, 3D and S2). These data demonstrate that LZTFL1 is a cilium protein that regulates the level of BBS9 in the primary cilium during physiological conditions.

2.3 LZTFL1 depletion causes progressive retinal degeneration in mice

Defects in some BBS genes, such as *Bbs4, Bbs2, Bbs3* and *Bbs7* are known to cause retinal degeneration in mouse model (Mykytyn et al., 2004; Nishimura et al., 2004; Zhang et al., 2011; Zhang et al., 2013), so we investigated the effect of *Lztfl1* knockout on retinal structure. Hematoxylin and eosin (H&E) staining of eye sections from 112-day-old mice showed retinal degeneration in knockout eye (Fig. 4A). Further H&E staining of retina sections from wild-type and *Lztfl1* knockout eyes at different ages showed that the retinal degeneration in knockout eyes was progressive with age (Fig. 4B). The outer nuclear layer's (ONL's) thickness began to show differences between the wild-type and knockout mice at

17 days after birth (DAB). Retinal degeneration continued from one to four months in the knockout mice, and the outer segment layer was almost absent by about 166 DAB. Other parts of the retina, including the inner nuclear layer (INL) and ganglion cell layer (GCL), appeared normal in knockout mice (Fig. 4B). Interestingly, the retinal structure from eye sections from 14-day-old *Lztfl1* knockout mice was similar to that from the wild-type mice (Fig. 4B); however, a close examination by transmission electron microscopy (TEM) showed that the outer segment of photoreceptor cells in a 14-day-old knockout mouse was dramatically shortened and disorganized, and had lost its orientation compared to its wild-type sibling. Swirling disk membranes and bubble-like structures were frequently seen in the knockout samples (Fig. 4C).

2.4 Mislocalization of rhodopsin and cell death in the retinas of the *Lztfl1* knockout mice

Rhodopsin is one of the most abundant proteins in the outer segment of photoreceptor cells (Bhowmick et al., 2009). Mislocalized rhodopsin triggers cell death through G-protein stimulation of adenylate cyclase, which elevates cAMP levels and leads to caspase-3 activation (Alfinito and Townes-Anderson, 2002). Since *Lztfl1*-null mice showed progressive retinal degeneration, we examined the rhodopsin localization and cell death in the retinas of 21-day-old wild-type and knockout mice. As expected, the rhodopsin was detected in the outer segment of the wild-type retina (Fig. 5A). However, in knockout mice, besides the outer segment, rhodopsin was also observed in the ONL (Fig. 5B), indicating that rhodopsin transportation was impaired when the LZTFL1 protein was depleted in the photoreceptor cells. Additionally, rhodopsin staining also demonstrated that the outer segments of the knockout retinas were thinner than those of the wild-type. Subsequently, the effect of rhodopsin mislocalization on photoreceptor cell apoptosis was examined by a terminal deoxynucleotidyl transferase dUTP nick-end labeling (TUNEL) assay. DNA fragmentation was observed in significant numbers of photoreceptor cells, as demonstrated by the fluorescent signals generated specifically from end-labeling nicked DNA in the ONL of the knockout mouse retinas (Fig. 5D). However, the TUNEL signals in the ONL from wild-type retinal tissues were barely detectable (Fig. 5C). To confirm the relationship between rhodopsin localization and apoptosis, we conducted the TUNEL assay and rhodopsin staining at the same time. The staining of wild-type ONL was negative for both apoptosis and rhodopsin (Fig. 5E). Interestingly, significant numbers of cells were individually stained by either of the two dyes, and only a small fraction of cells in the knockout mouse retinas were stained by both dyes (Fig. 5F). These data provided direct evidence that removing LZTFL1 from the mouse retinas results in rhodopsin mislocalization and photoreceptor cell apoptosis, consistent with the retinal degeneration phenotype.

2.5 Distortion of the distal axoneme of the photoreceptor connecting cilium in the absence of LZTFL1

The photoreceptor cell outer segment is a modified cilium that is significantly enlarged to accommodate a large amount of proteins responsible for photo-conversion and signal transduction (Wright et al., 2010). TEM analysis showed that the basal body structure and proximal connecting cilium of *Lztfl1* knockout mice were very similar to those of wild-type mice (Fig. 6). However, the extension portion of the connecting cilium in the knockout mouse retina was significantly truncated with enlarged axoneme (Fig. 6B–D). These

characteristics were first observed in approximately one-month-old knockout mice and were then confirmed with younger knockout mice at 14 DAB. The normal axoneme inner diameter is approximately 156.26 ± 4.85 nm in mice (Gilliam et al., 2012). However, in the *Lztfl1* knockout mice, the average axoneme inner diameter was 310 ± 18.08 nm, in contrast to 147 ± 12.39 nm for axonemes in wild-type mice (Fig. 6D). This finding was confirmed by the confocal microscopic examination of the connecting cilium stained with a fluorescent dye–conjugated acetylated tubulin antibody (Fig. S3). Instead of the normal rod-like tubulin bundle, knockout mouse retina had fork-like structures at the distal end of the connecting cilium (Fig. S3). Interestingly, vesicles were present in the middle of the distal connecting cilium of the knockout samples, which were not seen in the wild-type samples (Fig. 6D). These unusual features in the axoneme of the knockout photoreceptor connecting cilium could play a role in retinal degeneration.

2.6 LZTFL1 depletion alters the distribution of adaptor protein complex 1 (AP1) in the photoreceptor cells

Recently, AP1-deficient *Caenorhabditis elegans* worms were shown to be defective in cilium morphology, positioning, and orientation (Kaplan et al., 2010). Most importantly, the microtubules of the ciliary axoneme in this animal model were frequently missing or became dispersed at the distal end, indicating that AP1 plays a significant role in cilia assembly (Kaplan et al., 2010). Based on this information, the localization of AP1 in *Lztfl1* knockout mouse retinal tissues was examined by immunofluorescent staining and confocal microscopy. Results showed that in wild-type retinas the AP1 was present within the photoreceptor inner segments and in the cell body area surrounding the ONL (Fig. 7A). However, in the inner segment of the *Lztfl1* knockout retinas, a fraction of photoreceptor cells had higher level of AP1, while the rest of the cells had very low levels (Fig. 7B). To further characterize the role of AP1, photoreceptor cells were stained for AP1 and the cilium marker acetylated tubulin. Unlike in the wild-type, AP1 and acetylated tubulin were co-localized in some cells in the knockout retina (Fig. 7C and D). The altered distribution of AP1 in the retinas of the knockout mice suggests that LZTFL1 plays an important role in the canonical vesicle trafficking pathway.

3. Discussion

BBS is a genetically heterogeneous disease related to cilia dysfunction (Sheffield, 2010). Compromised cilium has been shown to be associated with a high incidence of diabetes and obesity (Oh et al., 2015), which are common phenotypes seen in *Bbs1, Bbs2, and Bbs4* knockout mice (Kim et al., 2004; Nishimura et al., 2004; Davis et al., 2007). Consistent with these reports, we observed that LZTFL1 (BBS17)-deficient mice gained more weight than their wild-type siblings. Data presented here and elsewhere (Seo et al., 2011) show that the absence of LZTFL1 results in an increased level of BBS in cilia. This increase could compromise ciliary function, leading to weight gain and obesity.

In human and rodent models, BBS protein deficiencies are also known to cause kidney defects (Nishimura et al., 2004; Guo et al., 2011; Imhoff et al., 2011;). However, in this study phenotypic characterization did not find significant differences in kidney tissues

between *Lztfl1* knockout and wild-type mice. Interestingly, LZTFL1 is localized in the primary cilium of wild-type mouse kidneys (Fig. 3), and the absence of LZTFL1 increases the level of BBS9 in the primary cilium, although not as much as reported for the hTERT-RPE1 cell line (Seo et al., 2011). These data suggest that BBSome complex's function in the primary cilium is not affected in the kidney of *Lztfl1* knockout mice, which is consistent with their normal kidney phenotype.

In a previous study, LZTFL1 was found in the cytoplasm, but not in the cilia or basal body, and LZTFL1 knockdown led to an accumulation of BBS proteins in the primary cilium (Seo et al., 2011). The reason for the contradiction of LZTFL1 localization between the results presented in this study and the results reported by Seo et al. is not known, but might be explained by the fact that different materials were used (human hTERT-RPE1 cell line used by Seo et al. and mouse kidney tissue used in the present study). It is noteworthy that species differences may also be a reason, as have been seen in other studies showing that BBS gene knockouts in mice result in different phenotypic outcomes compared to the corresponding gene mutations in humans, indicating that rodent disease models cannot completely duplicate human disorders (Davis et al., 2007; Zhang et al., 2014).

In *Lztfl1* knockout mouse photoreceptor cells, the axoneme structure of the connecting cilium is enlarged (Fig. 6). A similar phenomenon has been observed, but not analyzed in detail, in reports on IFT protein IFT88 and retinitis pigmentosa GTPase regulator–interacting protein 1 (Pazour et al., 2002; Patil et al., 2012). In this study, we have characterized this unusual phenotype in *Lztfl1*-null photoreceptor cells using TEM and compared it with the dimensions of a normal connecting cilium structure (Gilliam et al., 2012). AP1 has been found to regulate cilium formation, axonemal length, and microtubule arrangement in *C. elegans*, and *AP1* knockdown in human cells can impair cilium structure, orientation, and microtubule post-translational modification (Kaplan et al., 2010). Interestingly, we found that AP1 was abnormally distributed in some of the knockout mouse photoreceptor cells, suggesting that LZTFL1 has a role in AP1-mediated trafficking.

In summary, a knockout mouse model was used to investigate the physiological function of the LZTFL1 and the data showed that LZTFL1 is a ciliary protein that regulates mouse body weight and retinal function. Also, data presented here supported that LZTFL1 may play a critical role in maintaining the connecting cilium structure, and that it may serve as an intersection between the BBSome and AP1 pathways for the regulation of microtubule assembly and cilium protein trafficking. These data have implications for the role of this protein in human ciliopathy and related disorders.

4. Materials and Methods

4.1 Generation of *Lztfl1* knockout mice

Lztfl1$^{-/-}$ embryonic stem cells were obtained from the KOMP Repository (USA) and grown on gelatin-coated tissue-culture plates containing a layer of mouse embryonic fibroblasts (isolated from 15.5 days post-coitum (dpc) C57BL/6NCr fetuses). The cells were cultured in Resgro medium (EMD, Germany) at a density of 2.0×10^6 cells per 60-mm plate and passaged 1:3 every 48 h. Prior to microinjection, the embryonic stem cells were trypsinized

for 5 min using 0.05% trypsin with EDTA, supplemented with 1% chicken serum, washed and pelleted by centrifugation at 1000 r/min for 5 min followed by re-suspension in Resgro medium (EMD), and microinjected into C57BL/6NCr blastocysts. The resulting male chimeras were mated with C57BL/6NCr females to generate germline-transmitted progeny. Heterozygous mice (*Lztfl1*$^{+/-}$) were identified by PCR screening and mated at four weeks of age to generate homozygous knockout mice (*Lztfl1*$^{-/-}$). Due to compromised fertility in homozygous knockout mice, the colony was maintained by heterozygous crosses. All studies with mice adhered to the guidelines established for the care and use of experimental animals and were approved by the Animal Care and Use Committee of Leidos Biomedical Research, Inc.

4.2 Real-time quantitative RT-PCR

Total cellular RNA was extracted using the ISOLATE II RNA Mini kit (Bioline, USA). To quantitatively analyze gene expression, 250 ng of total RNA was used to synthesize the first-strand cDNA with random primers. The qRT-PCR was performed using SYBR Green Master Mix (Qiagen, USA), and the quantity of *Lztfl1* mRNA was normalized by the mRNA levels of glyceraldehyde-3-phosphate dehydrogenase.

4.3 Tissue harvesting, sectioning, and hematoxylin and eosin staining

Fresh tissues were fixed in 10% neutral buffered formalin (10% NBF; Fisher Scientific, USA) for a minimum of 48 h. Fixed tissues were processed with a Sakura 4894 tissue processor (Sakura, USA) according to the manufacturer's protocol and then embedded into paraffin blocks. Unstained sections were prepared with a Leica Model RM2255 rotary automated microtome (Leica, USA). Paraffin ribbons were cut at 5 μm and floated on a 37°C water bath, and then individual sections were mounted onto positively charged glass microscope slides (Fisher plus slides; Thermo-Fisher, USA) and allowed to air dry prior to staining. H&E staining was adapted from the Carson procedure onto a Sakura Tissue-Tek Prisma Automated Slide Stainer (Carson, 1997). Specifically, bake slides at 65°C for 10 min; deparaffinize in fresh Xylenes three times for 4 min each; rehydrate though graded ethanol: 100% for 2 min, 80% for 1.5 min, water for 1 min; stain with hematoxylin II for 5 min, water for 1 min, clarifier for 1 min, bluing agent for 1 min, water for 1 min, 95% ethanol for 1 min; stain with Eosin Y for 20 secs, 100% ethanol for 2 min, 100% ethanol three times for 3 min each; stain with Xylene three times for 3 min each; and mount coverslip with Permount. The resulting stained slides were digitally scanned with an Aperio model XT digital bright-field whole-slide scanner at 40× native resolution.

4.4 Transmission electron microscopy

The TEM method was based on previous study (Rachel et al., 2012). Briefly, the mouse eyes were surgically removed and fixed in a cocktail of 4% formaldehyde and 2% glutaraldehyde in a 0.1 M cacodylate buffer, and post-fixed in 1% osmium tetroxide. The sample was then dehydrated in a series of graded alcohols (35%, 50%, 70%, 95%, and 100%), after which the eyes were infiltrated overnight in a 1:1 mixture of propylene oxide and epoxy resin, and then embedded in pure resin and cured at 55°C for 48 h. The cured block was trimmed, and semi-thin sections (0.5 μm) were made and stained with Toluidine Blue solution to determine the proper orientation for electron microscope imaging. Thin sections (70–80 nm) were then

mounted on bare 200-mesh copper grids and subsequently stained in uranyl acetate and lead citrate. The sections were imaged utilizing a Hitachi H-7650 (Japan) transmission electron microscope equipped with an AMT (Danvers, USA) digital camera.

4.5 Immunofluorescent staining, TUNEL assay, and confocal microscopy

Antigen retrieval was carried out for the fixed tissue sections (5 μm), by following the manufacturer's instruction (S1700; Dako North America, Inc., USA). For staining, samples were first blocked in blocking buffer (5% goat serum, 1 × PBS, 0.5% Triton X-100) for 1 h. The primary antibody was diluted to 1:100–1:200 in the blocking buffer and incubated with the sample overnight at 4°C. The secondary antibody was diluted to 1:500 and incubated for 2 h after the primary antibody. After extensive wash, the slide was loaded with ProLong® Gold Antifade reagent with DAPI reagent (P-36931; Life Technologies, USA) and mounted. The following antibodies were used: rabbit polyclonal antibody against human BBS9 (1:100; Sigma, USA), see Fig. S1 for the evaluation of BBS9 antibody specificity for mouse tissue; mouse monoclonal antibody against acetylated tubulin (1:200; Sigma); rabbit polyclonal antibody against LZTFL1 (1:100; Sigma); mouse monoclonal antibody against AP1 (1:100; BD Transduction Laboratories, USA); mouse monoclonal antibody against rhodopsin (1:100; Santa Cruz Biotechnology, USA); goat monoclonal antibody against actin (1:500; Santa Cruz Biotechnology). Goat secondary antibodies were conjugated to Alexa Fluor 488, 568, and 647 (1:500; Molecular Probes, USA).

The TUNEL assay was conducted using the DeadEnd™ Fluorometric TUNEL System according to the manufacturer's instructions (G3250; Promega, USA). For TUNEL and rhodopsin dual staining, the tissue sections were first labeled using TUNEL and then stained with an antibody against rhodopsin. The slides were then mounted and imaged.

Images were acquired with a Zeiss 510 or 710 confocal microscope. Pictures were processed by Zen software or ImageJ. The BBS9 level was measured in 20 cilia each from wild-type and knockout mice kidneys. Specifically, confocal images were opened in the ImageJ software, an individual primary cilium in the kidneys was manually chosen, and the area was defined with the polygon selection tool. The signal intensity corresponding to the BBS9- and cilia-staining channels was measured. The blank area with the same size adjacent to each defined area was also recorded as background and subtracted from the recorded data. All data were plotted using GraphPad Prism 6 software and are shown as mean ± SEM. The inner diameters of connecting cilium were measured with ImageJ and statistically analyzed with GraphPad Prism 6 software.

4.6 Data analysis

Experiments were repeated at least three times unless otherwise stated. P values were calculated with the two-tailed t-test, using the GraphPad Prism software. Results were shown as mean ± SEM, with * representing significantly differences at $P < 0.05$. Images shown are representative of one of the three experiments.

Supplementary Material

Refer to Web version on PubMed Central for supplementary material.

Acknowledgments

This work has been funded in whole or in part with federal funds from the National Cancer Institute, National Institutes of Health, under contract [HHSN261200800001E]. The content of this publication does not necessarily reflect the views or policies of the Department of Health and Human Services, nor does mention of trade names, commercial products, or organizations imply endorsement by the U.S. Government. This research was supported by the National Institute of Allergy and Infectious Diseases. We would like to thank Kunio Nagashima for help with electron microscope analysis, as well as Mohammad Ishaq and other members of the Laboratory of Molecular Cell Biology for valuable suggestions.

References

Alfinito PD, Townes-Anderson E. Activation of mislocalized opsin kills rod cells: a novel mechanism for rod cell death in retinal disease. Proc. Natl. Acad. Sci. USA. 2002; 99:5655–5660. [PubMed: 11943854]

Avidor-Reiss T, Maer AM, Koundakjian E, Polyanovsky A, Keil T, Subramaniam S, Zuker CS. Decoding cilia function: defining specialized genes required for compartmentalized cilia biogenesis. Cell. 2004; 117:527–539. [PubMed: 15137945]

Berbari NF, Pasek RC, Malarkey EB, Yazdi SM, McNair AD, Lewis WR, Nagy TR, Kesterson RA, Yoder BK. Leptin resistance is a secondary consequence of the obesity in ciliopathy mutant mice. Proc. Natl. Acad. Sci. USA. 2013; 110:7796–7801. [PubMed: 23599282]

Bhogaraju S, Engel BD, Lorentzen E. Intraflagellar transport complex structure and cargo interactions. Cilia. 2013; 2:10. [PubMed: 23945166]

Bhowmick R, Li M, Sun J, Baker SA, Insinna C, Besharse JC. Photoreceptor IFT complexes containing chaperones, guanylyl cyclase 1 and rhodopsin. Traffic. 2009; 10:648–663. [PubMed: 19302411]

Carson, FL. Histotechnology: a self-instructional text. ASCP Press; 1997.

Davis RE, Swiderski RE, Rahmouni K, Nishimura DY, Mullins RF, Agassandian K, Philp AR, Searby CC, Andrews MP, Thompson S, Berry CJ, Thedens DR, Yang B, Weiss RM, Cassell MD, Stone EM, Sheffield VC. A knockin mouse model of the Bardet-Biedl syndrome 1 M390R mutation has cilia defects, ventriculomegaly, retinopathy, and obesity. Proc. Natl. Acad. Sci. USA. 2007; 104:19422–19427. [PubMed: 18032602]

Eguether T, San Agustin JT, Keady BT, Jonassen JA, Liang Y, Francis R, Tobita K, Johnson CA, Abdelhamed ZA, Lo CW, Pazour GJ. IFT27 links the BBSome to IFT for maintenance of the ciliary signaling compartment. Dev. Cell. 2014; 31:279–290. [PubMed: 25446516]

Forsythe E, Beales PL. Bardet-Biedl syndrome. Eur. J. Hum. Genet. 2013; 21:8–13. [PubMed: 22713813]

Gilliam JC, Chang JT, Sandoval IM, Zhang Y, Li T, Pittler SJ, Chiu W, Wensel TG. Three-dimensional architecture of the rod sensory cilium and its disruption in retinal neurodegeneration. Cell. 2012; 151:1029–1041. [PubMed: 23178122]

Guo DF, Beyer AM, Yang B, Nishimura DY, Sheffield VC, Rahmouni K. Inactivation of Bardet-Biedl syndrome genes causes kidney defects. Am. J. Physiol. Renal Physiol. 2011; 300:F574–F580. [PubMed: 21106857]

Imhoff O, Marion V, Stoetzel C, Durand M, Holder M, Sigaudy S, Sarda P, Hamel CP, Brandt C, Dollfus H, Moulin B. Bardet-Biedl syndrome: a study of the renal and cardiovascular phenotypes in a French cohort. Clin. J. Am. Soc. Nephrol. 2011; 6:22–29. [PubMed: 20876674]

Jin H, White SR, Shida T, Schulz S, Aguiar M, Gygi SP, Bazan JF, Nachury MV. The conserved Bardet-Biedl syndrome proteins assemble a coat that traffics membrane proteins to cilia. Cell. 2010; 141:1208–1219. [PubMed: 20603001]

Kang SG, Park J, Cho JY, Ulrich B, Kim CH. Complementary roles of retinoic acid and TGF-beta1 in coordinated expression of mucosal integrins by T cells. Mucosal Immunol. 2011; 4:66–82. [PubMed: 20664575]

Kaplan OI, Molla-Herman A, Cevik S, Ghossoub R, Kida K, Kimura Y, Jenkins P, Martens JR, Setou M, Benmerah A, Blacque OE. The AP-1 clathrin adaptor facilitates cilium formation and functions

with RAB 8 in *C. elegans* ciliary membrane transport. J. Cell Sci. 2010; 123:3966–3977. [PubMed: 20980383]

Kim JC, Badano JL, Sibold S, Esmail MA, Hill J, Hoskins BE, Leitch CC, Venner K, Ansley SJ, Ross AJ, Leroux MR, Katsanis N, Beales PL. The Bardet-Biedl protein BBS4 targets cargo to the pericentriolar region and is required for microtubule anchoring and cell cycle progression. Nat. Genet. 2004; 36:462–470. [PubMed: 15107855]

Kiss H, Kedra D, Kiss C, Kost-Alimova M, Yang Y, Klein G, Imreh S, Dumanski JP. The *LZTFL1* gene is a part of a transcriptional map covering 250 kb within the common eliminated region 1 (C3CER1) in 3p21.3. Genomics. 2001; 73:10–19. [PubMed: 11352561]

Kulaga HM, Leitch CC, Eichers ER, Badano JL, Lesemann A, Hoskins BE, Lupski JR, Beales PL, Reed RR, Katsanis N. Loss of BBS proteins causes anosmia in humans and defects in olfactory cilia structure and function in the mouse. Nat. Genet. 2004; 36:994–998. [PubMed: 15322545]

Lee JH, Ulrich B, Cho J, Park J, Kim CH. Progesterone promotes differentiation of human cord blood fetal T cells into T regulatory cells but suppresses their differentiation into Th17 cells. J. Immunol. 2011; 187:1778–1787. [PubMed: 21768398]

Marion V, Mockel A, De Melo C, Obringer C, Claussmann A, Simon A, Messaddeq N, Durand M, Dupuis L, Loeffler JP, King P, Mutter-Schmidt C, Petrovsky N, Stoetzel C, Dollfus H. BBS-induced ciliary defect enhances adipogenesis, causing paradoxical higher-insulin sensitivity, glucose usage, and decreased inflammatory response. Cell Metab. 2012a; 16:363–377. [PubMed: 22958920]

Marion V, Stutzmann F, Gerard M, De Melo C, Schaefer E, Claussmann A, Helle S, Delague V, Souied E, Barrey C, Verloes A, Stoetzel C, Dollfus H. Exome sequencing identifies mutations in LZTFL1, a BBSome and smoothened trafficking regulator, in a family with Bardet-Biedl syndrome with *situs inversus* and insertional polydactyly. J. Med. Genet. 2012b; 49:317–321. [PubMed: 22510444]

Mykytyn K, Mullins RF, Andrews M, Chiang AP, Swiderski RE, Yang B, Braun T, Casavant T, Stone EM, Sheffield VC. Bardet-Biedl syndrome type 4 (BBS4)-null mice implicate Bbs4 in flagella formation but not global cilia assembly. Proc. Natl. Acad. Sci. USA. 2004; 101:8664–8669. [PubMed: 15173597]

Nachury MV. How do cilia organize signalling cascades? Philos. Trans. R. Soc. B Biol. Sci. 2014; 369:20130465.

Nachury MV, Loktev AV, Zhang Q, Westlake CJ, Peranen J, Merdes A, Slusarski DC, Scheller RH, Bazan JF, Sheffield VC, Jackson PK. A core complex of BBS proteins cooperates with the GTPase Rab8 to promote ciliary membrane biogenesis. Cell. 2007; 129:1201–1213. [PubMed: 17574030]

Nishimura DY, Fath M, Mullins RF, Searby C, Andrews M, Davis R, Andorf JL, Mykytyn K, Swiderski RE, Yang B, Carmi R, Stone EM, Sheffield VC. *Bbs2*-null mice have neurosensory deficits, a defect in social dominance, and retinopathy associated with mislocalization of rhodopsin. Proc. Natl. Acad. Sci. USA. 2004; 101:16588–16593. [PubMed: 15539463]

Oh EC, Vasanth S, Katsanis N. Metabolic regulation and energy homeostasis through the primary Cilium. Cell Metab. 2015; 21:21–31. [PubMed: 25543293]

Pampliega O, Orhon I, Patel B, Sridhar S, Diaz-Carretero A, Beau I, Codogno P, Satir BH, Satir P, Cuervo AM. Functional interaction between autophagy and ciliogenesis. Nature. 2013; 502:194–200. [PubMed: 24089209]

Patil H, Tserentsoodol N, Saha A, Hao Y, Webb M, Ferreira PA. Selective loss of RPGRIP1-dependent ciliary targeting of NPHP4, RPGR and SDCCAG8 underlies the degeneration of photoreceptor neurons. Cell Death Dis. 2012; 3:e355. [PubMed: 22825473]

Pazour GJ, Baker SA, Deane JA, Cole DG, Dickert BL, Rosenbaum JL, Witman GB, Besharse JC. The intraflagellar transport protein, IFT88, is essential for vertebrate photoreceptor assembly and maintenance. J. Cell Biol. 2002; 157:103–113. [PubMed: 11916979]

Pedersen LB, Christensen ST. Regulating intraflagellar transport. Nat. Cell Biol. 2012; 14:904–906. [PubMed: 22945257]

Pigino G, Geimer S, Lanzavecchia S, Paccagnini E, Cantele F, Diener DR, Rosenbaum JL, Lupetti P. Electron-tomographic analysis of intraflagellar transport particle trains *in situ*. J. Cell Biol. 2009; 187:135–148. [PubMed: 19805633]

Rachel RA, Nagashima K, O'Sullivan TN, Frost LS, Stefano FP, Marigo V, Boesze-Battaglia K. Melanoregulin, product of the dsu locus, links the BLOC-pathway and OA1 in organelle biogenesis. PLoS One. 2012; 7:e42446. [PubMed: 22984402]

Sakurai T, Ogasawara J, Kizaki T, Ishibashi Y, Fujiwara T, Akagawa K, Izawa T, Oh-ishi S, Haga S, Ohno H. Involvement of leucine zipper transcription factor-like protein 1 (Lztfl1) in the attenuation of cognitive impairment by exercise training. Biochem. Biophys. Res. Commun. 2011; 416:125–129. [PubMed: 22093827]

Schaefer E, Lauer J, Durand M, Pelletier V, Obringer C, Claussmann A, Braun JJ, Redin C, Mathis C, Muller J, Schmidt-Mutter C, Flori E, Marion V, Stoetzel C, Dollfus H. Mesoaxial polydactyly is a major feature in Bardet-Biedl syndrome patients with LZTFL1 (BBS17) mutations. Clin. Genet. 2014; 85:476–481. [PubMed: 23692385]

Scholey JM. Intraflagellar transport motors in cilia: moving along the cell's antenna. J. Cell Biol. 2008; 180:23–29. [PubMed: 18180368]

Seo S, Zhang Q, Bugge K, Breslow DK, Searby CC, Nachury MV, Sheffield VC. A novel protein LZTFL1 regulates ciliary trafficking of the BBSome and Smoothened. PLoS Genet. 2011; 7:e1002358. [PubMed: 22072986]

Sheffield VC. The blind leading the obese: the molecular pathophysiology of a human obesity syndrome. Trans. Am. Clin. Climatol. Assoc. 2010; 121:172–181. discussion 181-172. [PubMed: 20697559]

Tang Z, Lin MG, Stowe TR, Chen S, Zhu M, Stearns T, Franco B, Zhong Q. Autophagy promotes primary ciliogenesis by removing OFD1 from centriolar satellites. Nature. 2013; 502:254–257. [PubMed: 24089205]

Taschner M, Bhogaraju S, Vetter M, Morawetz M, Lorentzen E. Biochemical mapping of interactions within the intraflagellar transport (IFT) B core complex: IFT52 binds directly to four other IFT-B subunits. J. Biol. Chem. 2011; 286:26344–26352. [PubMed: 21642430]

van Dam TJ, Townsend MJ, Turk M, Schlessinger A, Sali A, Field MC, Huynen MA. Evolution of modular intraflagellar transport from a coatomer-like progenitor. Proc. Natl. Acad. Sci. USA. 2013; 110:6943–6948. [PubMed: 23569277]

Wei Q, Zhang Y, Li Y, Zhang Q, Ling K, Hu J. The BBSome controls IFT assembly and turnaround in cilia. Nat. Cell Biol. 2012; 14:950–957. [PubMed: 22922713]

Wei Q, Zhou W, Wang W, Gao B, Wang L, Cao J, Liu ZP. Tumor-suppressive functions of leucine zipper transcription factor-like 1. Cancer Res. 2010; 70:2942–2950. [PubMed: 20233871]

Williams CL, McIntyre JC, Norris SR, Jenkins PM, Zhang L, Pei Q, Verhey K, Martens JR. Direct evidence for BBSome-associated intraflagellar transport reveals distinct properties of native mammalian cilia. Nat. Commun. 2014; 5:5813. [PubMed: 25504142]

Wright AF, Chakarova CF, Abd El-Aziz MM, Bhattacharya SS. Photoreceptor degeneration: genetic and mechanistic dissection of a complex trait. Nat. Rev. Genet. 2010; 11:273–284. [PubMed: 20212494]

Yen HJ, Tayeh MK, Mullins RF, Stone EM, Sheffield VC, Slusarski DC. Bardet-Biedl syndrome genes are important in retrograde intracellular trafficking and Kupffer's vesicle cilia function. Hum. Mol. Genet. 2006; 15:667–677. [PubMed: 16399798]

Zhang Q, Nishimura D, Seo S, Vogel T, Morgan DA, Searby C, Bugge K, Stone EM, Rahmouni K, Sheffield VC. Bardet-Biedl syndrome 3 (Bbs3) knockout mouse model reveals common BBS-associated phenotypes and Bbs3 unique phenotypes. Proc. Natl. Acad. Sci. USA. 2011; 108:20678–20683. [PubMed: 22139371]

Zhang Q, Nishimura D, Vogel T, Shao J, Swiderski R, Yin T, Searby C, Carter CS, Kim G, Bugge K, Stone EM, Sheffield VC. BBS7 is required for BBSome formation and its absence in mice results in Bardet-Biedl syndrome phenotypes and selective abnormalities in membrane protein trafficking. J. Cell Sci. 2013; 126:2372–2380. [PubMed: 23572516]

Zhang Y, Seo S, Bhattarai S, Bugge K, Searby CC, Zhang Q, Drack AV, Stone EM, Sheffield VC. BBS mutations modify phenotypic expression of CEP290-related ciliopathies. Hum. Mol. Genet. 2014; 23:40–51. [PubMed: 23943788]

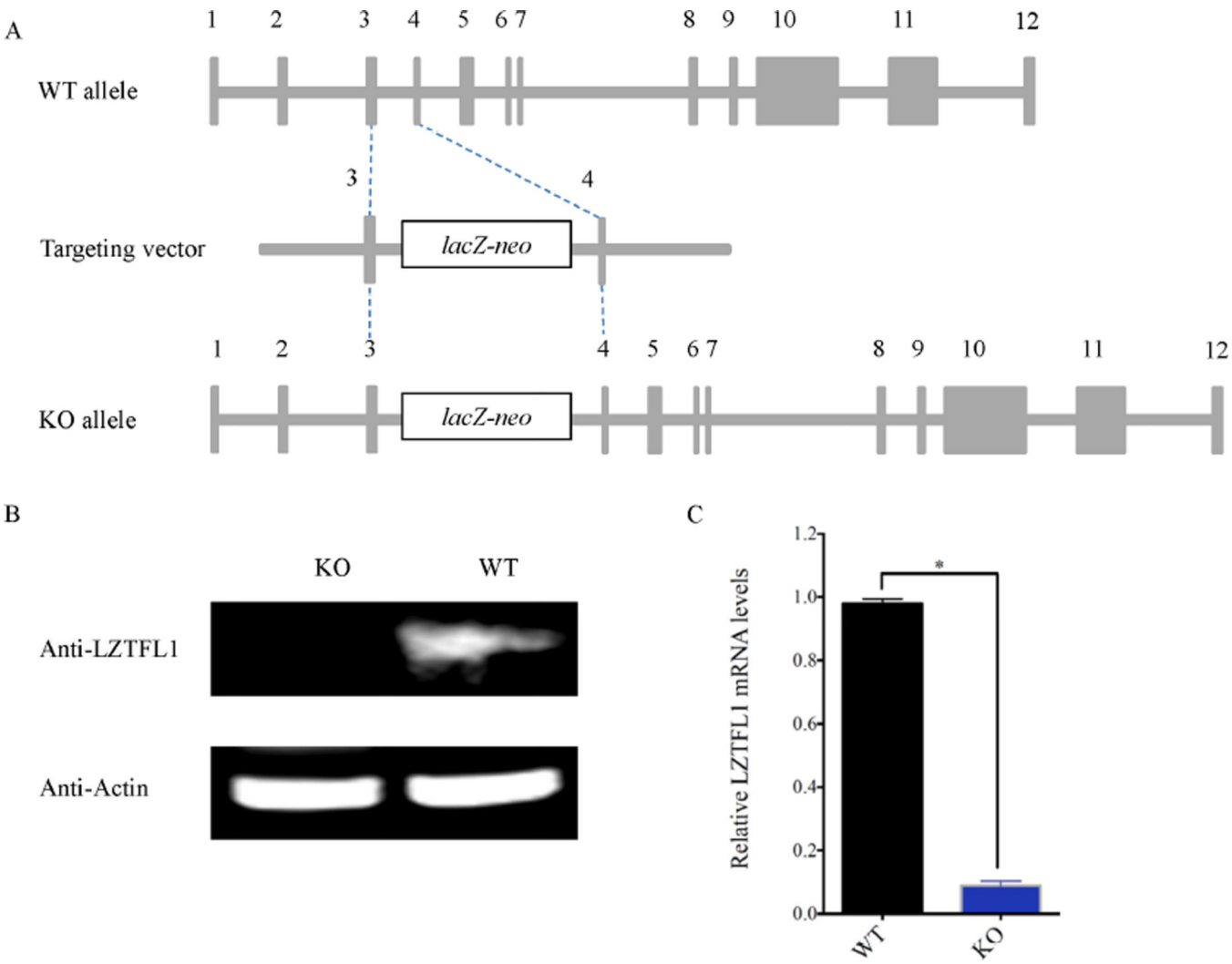

Fig. 1. Generation of *Lztfl1* knockout mouse line

A: Structures of *Lztfl1* targeting vector and wild-type and *Lztfl1* knockout alleles. After homologous recombination, a *LacZ-neo* cassette was inserted between exon 3 and exon 4 of *Lztfl1*. **B:** Western blot analysis showed the absence of LZTFL1 in *Lztfl1* knockout mice. Proteins were extracted from the wild-type and *Lztfl1* knockout mouse kidneys, respectively. Actin was used as a loading control. **C:** qRT-PCR analysis of *Lztfl1* mRNA expression in wild-type and *Lztfl1* knockout mouse kidneys, respectively. WT, wild-type; KO, knockout.

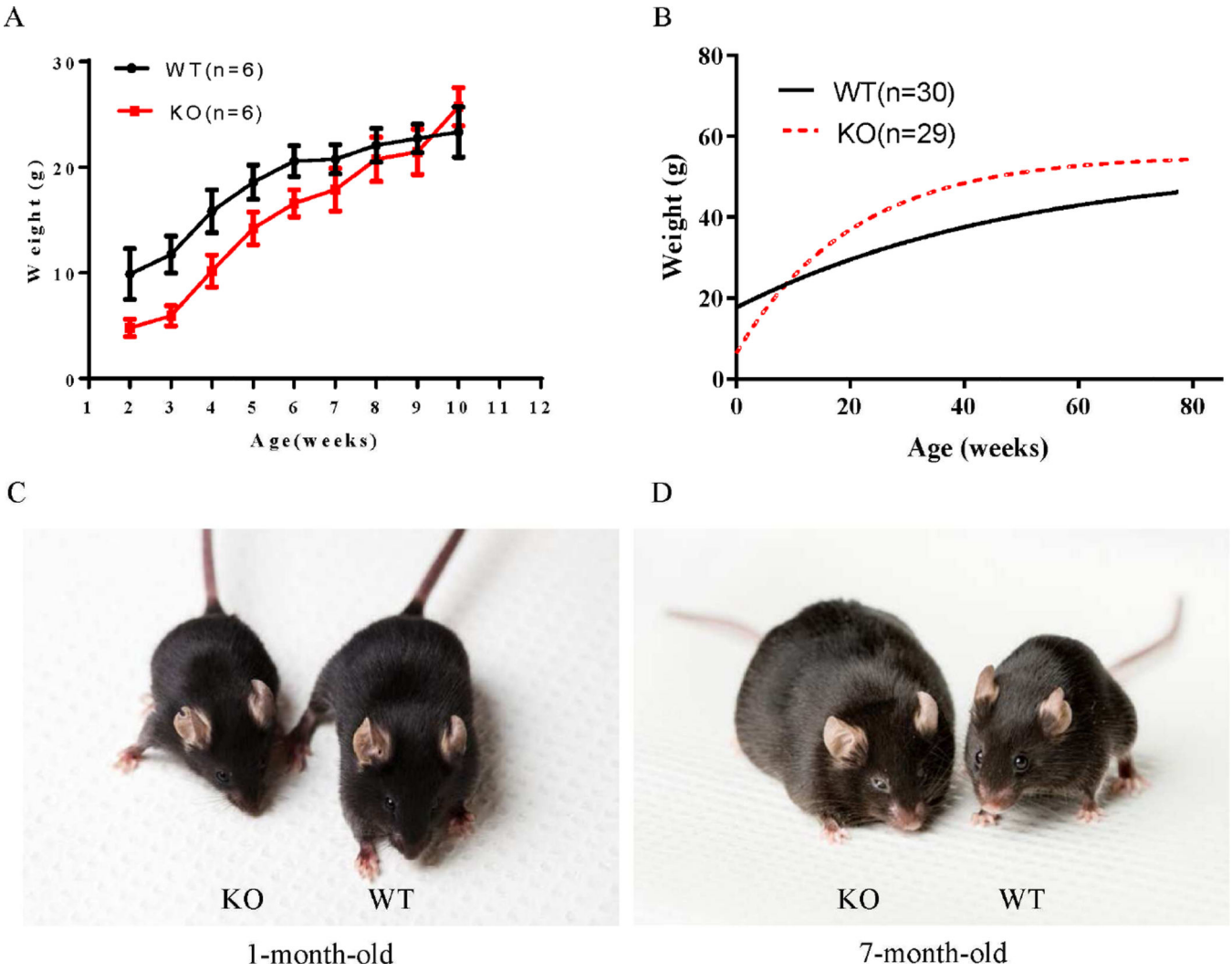

Fig. 2. *Lztfl1*-null mice gain more weight than wild-type mice with age

A and **B:** Growth curves of wild-type and *Lztfl1* knockout mice. **A:** *Lztfl1* knockout mice weighed less than their wild-type counterparts at birth, but reached similar weight to wild-type mice by approximately 10 weeks of age. Data are shown as mean ± SEM, $P < 0.01$. **B:** *Lztfl1* knockout mice gained more weight than their wild-type counterparts over their lifetimes. Wild-type and *Lztfl1* knockout mice were weighed at all ages. The curves were plotted using non-linear regression method with statistical correlation analysis, $P < 0.01$. **C** and **D:** Comparison of wild-type and *Lztfl1* knockout mice at different ages. WT, wild-type; KO, knockout.

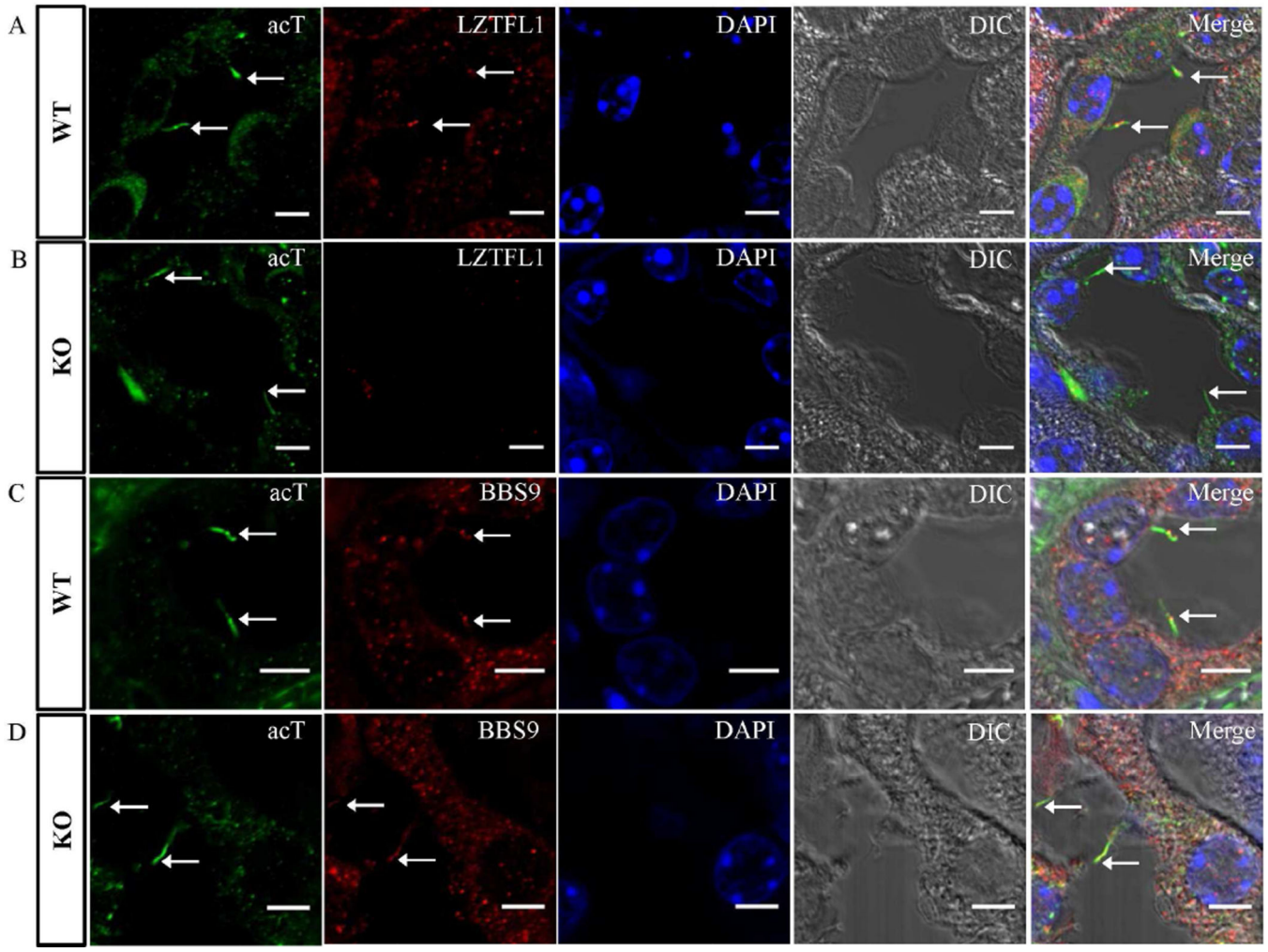

Fig. 3. LZTFL1 localizes in the primary cilium of the kidney and regulates BBS9

A and **B:** Kidney tissues from wild-type (**A**) and *Lztfl1* knockout (**B**) mice were immunostained with antibodies against acetylated tubulin (acT, green) and LZTFL1 (red) in the primary cilium. Bars = 5 μm. **C** and **D**: Kidney tissues from wild-type (**C**) and *Lztfl1* knockout (**D**) mice were immunostained with antibodies against acetylated tubulin (acT, green) and BBS9 (red) in the primary cilium. Bars = 5 μm. In **A–D**, cell nuclei were counterstained with DAPI, and the arrows indicate the primary cilia. WT, wild-type. KO, knockout.

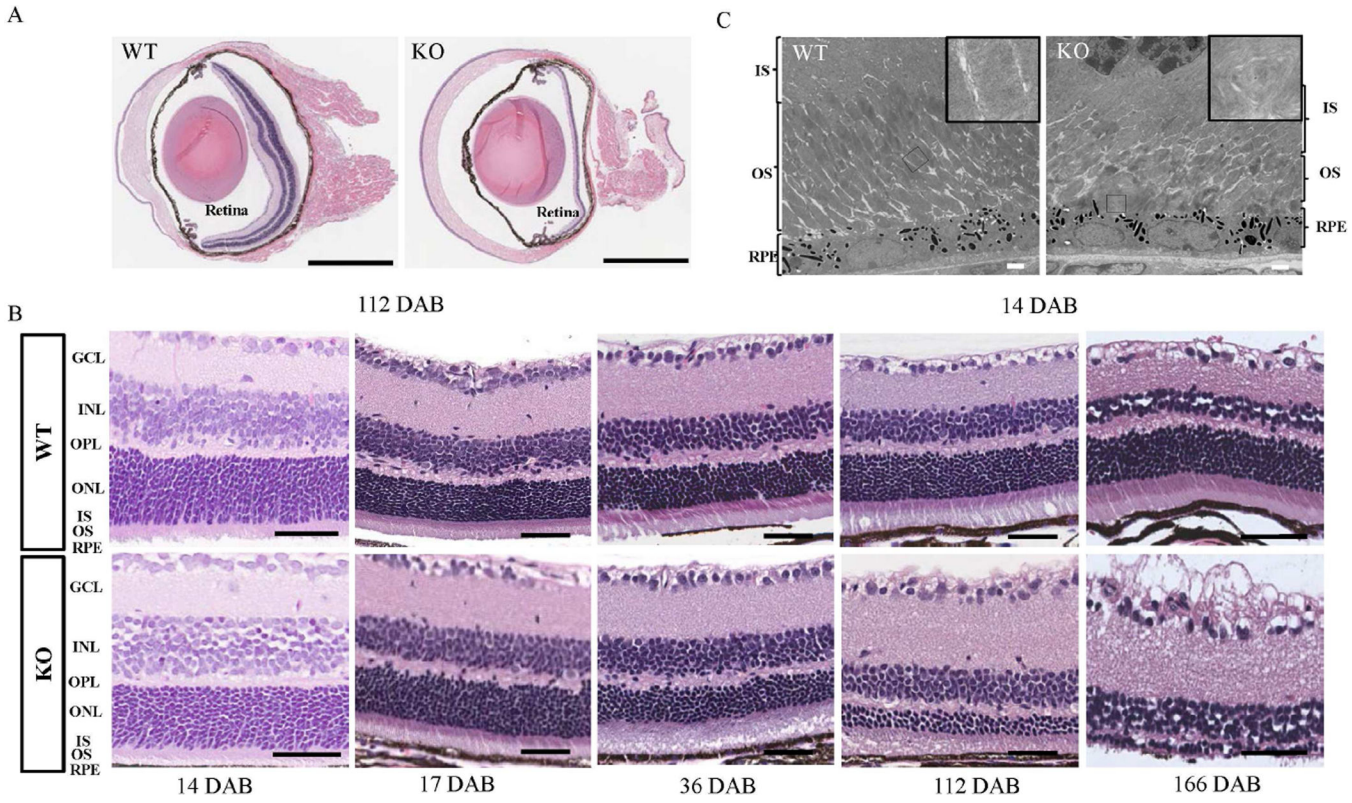

Fig. 4. Progressive retinal degeneration in *Lztfl1*-null mice

A: Hematoxylin and eosin staining of 112-day-old wild-type and *Lztfl1* knockout retinas, respectively. Bars = 1 mm. **B:** Progressive retinal degeneration in *Lztfl1* knockout mice. The thickness of knockout mice retinas was slightly different from that of wild type at 17 DAB. Bars = 50 μm. The photoreceptor cell layer is mostly degenerated by about 6 months in knockout mice retinas. Experiments were repeated twice, and representative images were shown. **C:** TEM analysis of 14-day-old wild-type and *Lztfl1* knockout retinas, respectively. The outer segment of the photoreceptor cells in the knockout retina is disoriented and fragmented, and the disc structure is disorganized with occasional swirls (inlet). Bars = 2 μm. IS, inner segment; OS, outer segment; RPE, retinal pigment epithelium; GCL, ganglion cell layer; INL, inner nuclear layer; OPL, outer plexiform layer; ONL, outer nuclear layer; DAB, days after birth; WT, wild-type; KO, knockout.

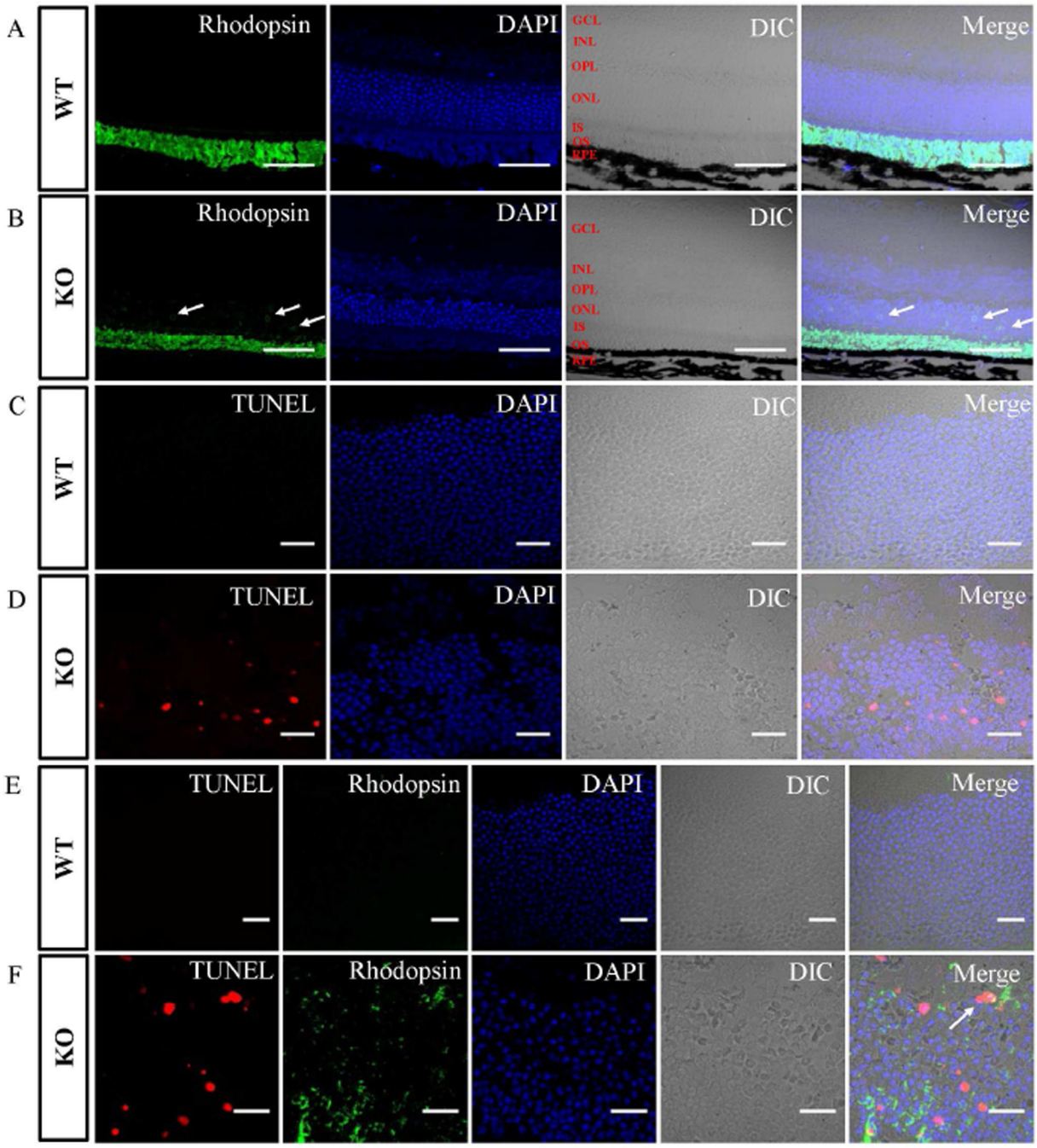

Fig 5. Mislocalized rhodopsin and increased apoptosis in *Lztfl1* knockout mouse retinas

A and **B**: Localization of rhodopsin in 21-day-old wild-type (**A**) and *Lztfl1* knockout (**B**) mouse retinas. The rhodopsin signal (green) appears in the outer segment of wild-type mouse retinas, whereas the signal occurs not only in the in the outer segment but also in the ONL surrounding the nuclei (arrows) in the knockout sample. Bars = 50 μm. **C** and **D:** The TUNEL assay showed apoptosis in the photoreceptor cells in *Lztfl1* knockout mouse retinas. Fragmented DNA was stained with a fluorescent dye (red) in retinal tissues. Bars = 20 μm. **E** and **F:** Simultaneous detection of rhodopsin (green) and apoptosis (red) in the ONL of wild-

type and *Lztfl1* knockout mouse retinas. Arrow shows the co-existence of TUNEL- and rhodopsin-staining signals in a small fraction of the photoreceptor cells in the knockout sample. Bars = 20 μm. GCL, ganglion cell layer; INL, inner nuclear layer; OPL, outer plexiform layer; ONL, outer nuclear layer; IS, inner segment; OS, outer segment; RPE, retinal pigment epithelium; WT, wild-type; KO, knockout.

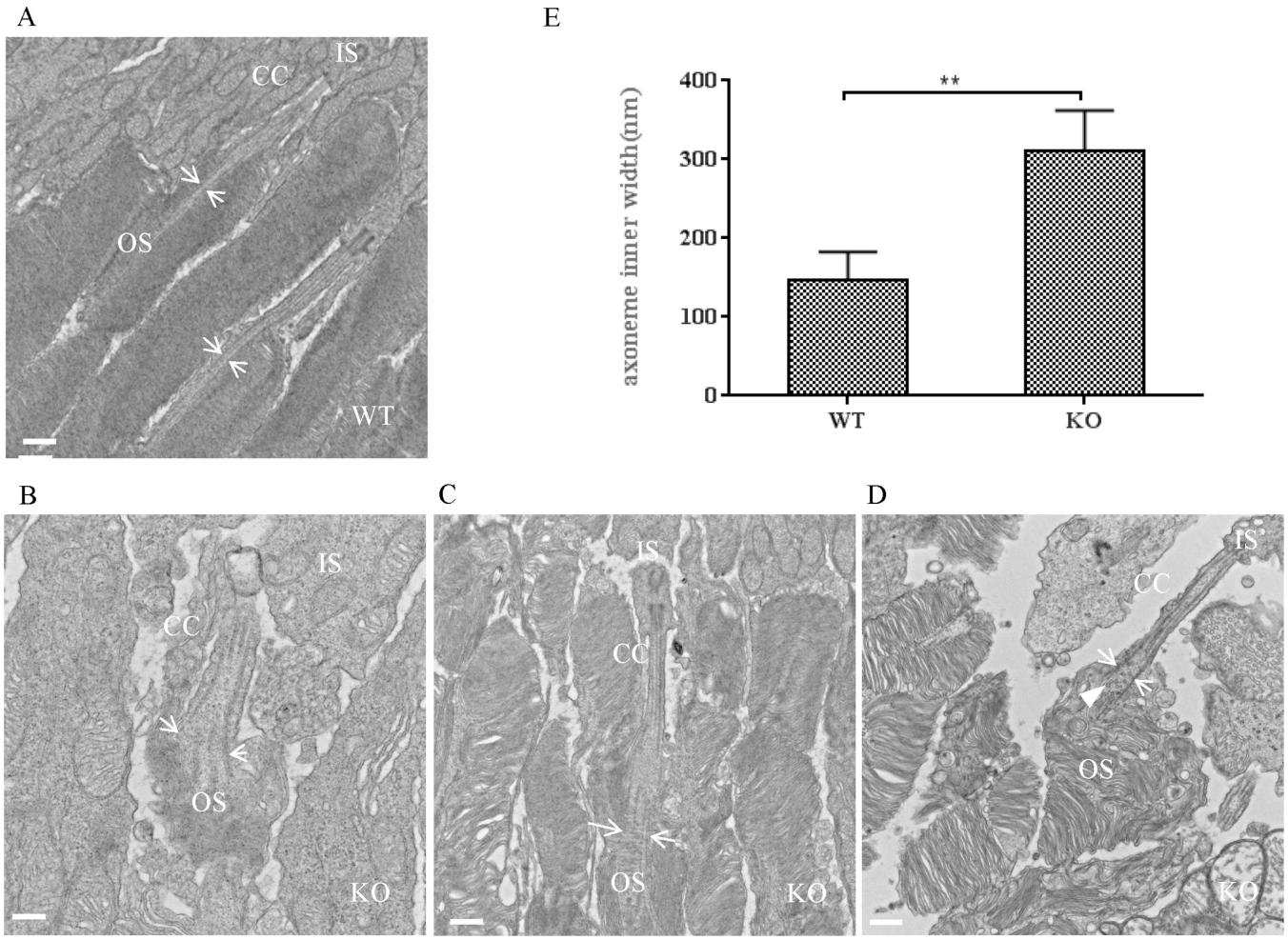

Fig. 6. The connecting cilium structure is modified in *Lztfl1* knockout mouse retinas

A–D: TEM characterization of wild-type (**A**) and *Lztfl1* knockout (**B–D**) photoreceptor cells. The microtubule bundle of the distal axoneme was enlarged in the connecting cilium of knockout mice (arrows in **B–D**), compared to the wild-type photoreceptor cells (arrows in **A**). Some vesicles were visible in the open axoneme (arrowhead in **D**). Bars = 500 nm. **E:** Comparison of the inner width of the distal axoneme between wild-type and *Lztfl1* knockout photoreceptor cells. The inner width (distance between the arrow pair) was measured from images generated by TEM (**A–D**). ** represents significant differences at $P < 0.01$ (Student's *t*-test). OS, outer segment; IS, inner segment; CC, connecting cilium; WT, wild-type; KO, knockout.

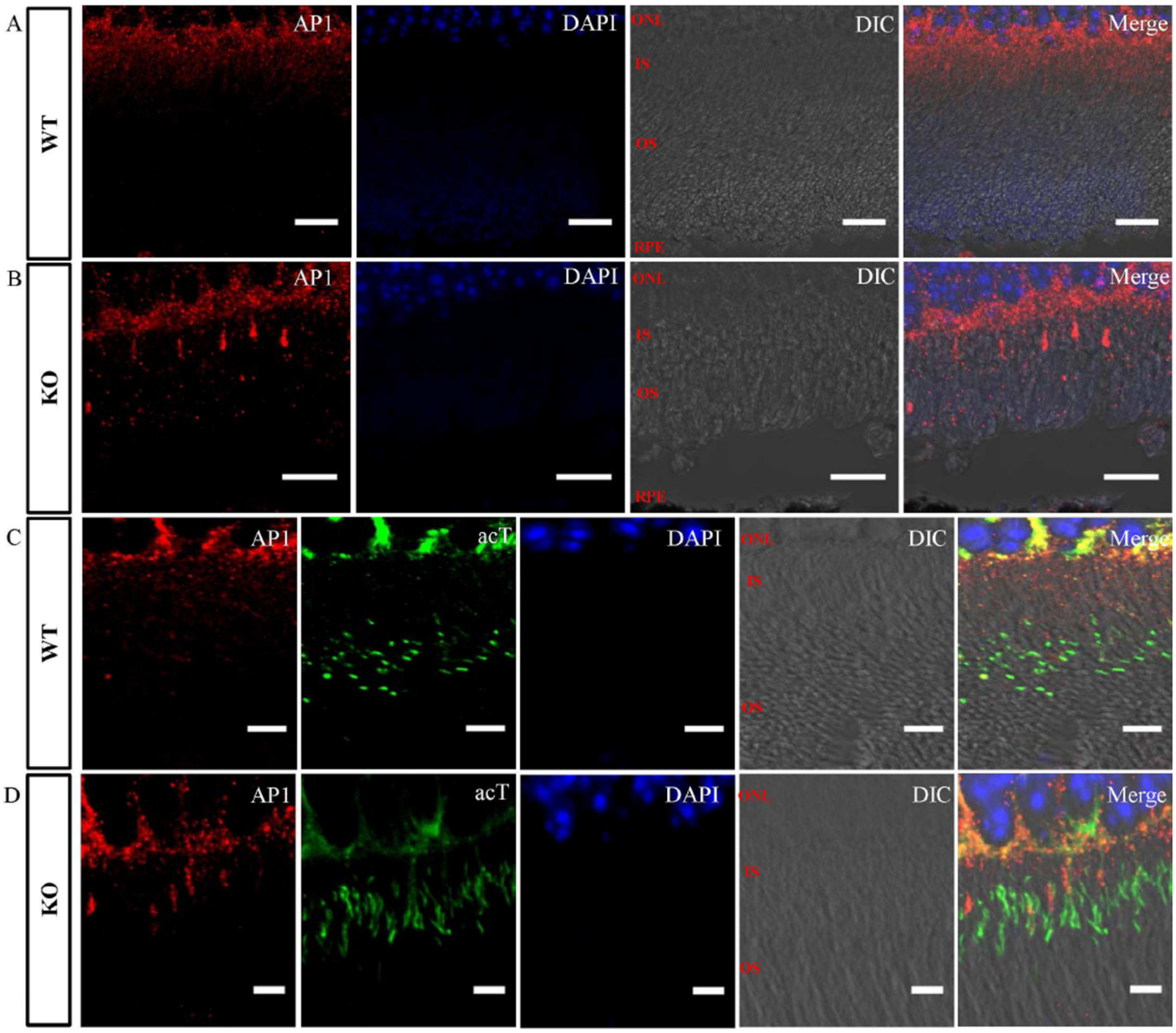

Fig. 7. Mislocalization of the AP1 in *Lztfl1* knockout mouse retina

Immunofluorescent staining of photoreceptor cells in retinas from wild-type (**A** and **C**) and *Lztfl1* knockout (**B** and **D**) mice with antibodies against AP1 (red, **A–D**) and acetylated tubulin (acT, green, **C** and **D**). AP1 was present in the inner segment of all wild-type photoreceptor cells (**A**). However, it was found to be highly enriched only in some of the photoreceptor cells in *Lztfl1*$^{-/-}$ mice (**B**). Acetylated tubulin and AP1 co-staining showed that the abnormally enriched AP1 in knockout photoreceptor cells was partially associated with the major connecting cilium structure (**D**). WT, wild-type; KO, knockout.